

Structural and mechanistic insights into Mcm2-7 double-hexamer assembly and function

Jingchuan Sun^{1,5}, Alejandra Fernandez-Cid^{2,5}, Alberto Riera^{2,5}, Silvia Tognetti², Zuanning
Yuan³, Bruce Stillman⁴, Christian Speck², Huilin Li^{1,3}

¹Biosciences Department, Brookhaven National Laboratory, Upton NY 11973, USA

²DNA Replication Group, MRC Clinical Sciences Centre, Imperial College Faculty of Medicine,
Hammersmith Hospital Campus, Du Cane Rd., London W12 0NN, UK

³Department of Biochemistry & Cell Biology, Stony Brook University, Stony Brook, NY 11794,

⁴Cold Spring Harbor Laboratory, 1 Bungtown Road, Cold Spring Harbor, NY 11724, USA

USA

⁵These authors contributed equally to this work

Correspondence and requests for materials should be addressed to

B.S. (stillman@cshl.edu), C.S. (chris.speck@csc.mrc.ac.uk), or H.L. (hli@bnl.gov).

Running head:

Key intermediates in pre-RC formation

Keywords:

Origin recognition complex, DNA replication initiation, Replicative helicase, pre-replication
complex, electron microscopy

Eukaryotic cells license each DNA replication origin during G1 phase by assembling a pre-replication complex that contains a Mcm2-7 double hexamer. During S phase, each Mcm2-7 hexamer forms the core of a replicative DNA helicase. However, the mechanisms of origin licensing and helicase activation are poorly understood. The helicase loaders ORC-Cdc6 function to recruit a single Cdt1-Mcm2-7 heptamer to replication origins, prior to Cdt1 release and ORC-Cdc6-Mcm2-7 complex formation, but how the second Mcm2-7 hexamer is recruited to promote double-hexamer formation is not well understood. Here, structural evidence for intermediates consisting of an ORC-Cdc6-Mcm2-7 complex and an ORC-Cdc6-Mcm2-7-Mcm2-7 complex are reported, which together provide new insights into DNA licensing. Detailed structural analysis of the loaded Mcm2-7 double-hexamer complex demonstrates that the two hexamers are interlocked and misaligned along the DNA axis and lack ATP-hydrolysis activity that is essential for DNA helicase activity. Moreover, we show that the head-to-head juxtaposition of the Mcm2-7 double-hexamer generates a new protein-interaction surface that creates a multi-subunit binding site for an S-phase protein kinase that is known to activate DNA replication. The data suggests how the double-hexamer is assembled and how helicase activity is regulated during DNA licensing, with implications for cell cycle control of DNA replication and genome stability.

DNA licensing is the focal point of several redundant cell cycle controls that guarantees each genome segment is replicated once and only once per cell division cycle (Bell and Dutta 2002; Remus and Diffley 2009; Pospiech et al. 2010; Siddiqui et al. 2013). The molecular basis of origin licensing has been best studied using the budding yeast *Saccharomyces cerevisiae* system. It involves assembly of a pre-Replicative Complex (pre-RC) by loading of the core replicative helicase Mini-Chromosome Maintenance proteins 2-7 (Mcm2-7) as a double hexamer around double-stranded (ds) DNA at each replication origin (Evrin et al. 2009; Remus et al. 2009). While in bacteria, archaea and eukaryotic viruses the loaded helicase is active for DNA unwinding, in eukaryotic cells the helicase is loaded in an inactive form (Yardimci and Walter 2014). This is a central feature for the temporal separation of DNA licensing in G1-phase from initiation of DNA replication in S-phase that is essential for once per cell cycle DNA replication (Diffley 2001). However, what confines the Mcm2-7 double-hexamer to its inactive state in G1-phase is only partially understood, but of relevance, as untimely helicase activation could result in re-replication and genomic instability.

Mcm2-7 double-hexamer formation is a multi-step reaction during which two Mcm2-7 hexamers are recruited one after another to replication origins (Evrin et al. 2013; Fernandez-Cid et al. 2013; Frigola et al. 2013). In *Saccharomyces cerevisiae* ORC-Cdc6 recognizes the replication origin in an ATP dependent manner (Bell and Stillman 1992; Speck et al. 2005; Speck and Stillman 2007) (**Figure 1A**, step 1). Chromatin bound ORC-Cdc6 function to recruit a Cdt1-Mcm2-7 heptamer to replication origins (Speck et al. 2005; Randell et al. 2006; Speck and Stillman 2007; Tsakraklides and Bell 2010; Evrin et al. 2013; Frigola et al. 2013; Sun et al. 2013) (**Figure 1A**, step 2). Using an *in vitro* Mcm2-7 loading system that employs purified ORC, Cdc6, Cdt1, Mcm2-7 hexamer and an origin-containing plasmid, we recently observed formation

of a loading intermediate termed OCCM in the presence of a slowly hydrolysable ATP analogue, ATP- γ S, which captured a complex containing ORC-Cdc6 bound to a single Mcm2-7 hexamer and 1-2 copies of Cdt1 (Takara and Bell 2011; Evrin et al. 2013; Sun et al. 2013). A Cryo-electron microscopy (EM) structure of this pre-RC intermediate showed that the AAA+ ATPase domains of ORC/Cdc6 latch onto the C-terminal AAA+ ATPase domains of Mcm2-7, leaving the Mcm2-7 N-terminal domains accessible, detailing the overall architecture of this important complex. Using biochemical experiments we observed that Orc1 and Cdc6 ATP-hydrolysis promotes rapid Cdt1 release and the formation of an ORC-Cdc6-Mcm2-7 (OCM) complex (Randell et al. 2006; Fernandez-Cid et al. 2013). One question that arises from that study is whether ATP hydrolysis by ORC-Cdc6 and subsequent Cdt1 dissociation leads to a resetting of ORC-Cdc6 on DNA such that it would be in a position to recruit the next Mcm2-7 hexamer (**Figure 1A**, step 3 right) or whether the ORC-Cdc6 stays tightly associated with the first Mcm2-7 hexamer (**Figure 1A**, step 3 left)? It is clear that the OCM complex is a precursor of Mcm2-7 double-hexamer formation (Fernandez-Cid et al. 2013), but how exactly the second Mcm2-7 hexamer becomes recruited is not known (**Figure 1A**, step 4) (Yardimci and Walter 2014). The final product of pre-RC formation is the Mcm2-7 double-hexamer (Evrin et al. 2009; Remus et al. 2009) and in this complex both hexamers interact via their N-termini (**Figure 1A**, step 5) (Remus et al. 2009; On et al. 2014). While pre-RC intermediates are salt sensitive, potentially because the Mcm2-7 ring becomes destabilized, the Mcm2-7 double-hexamer remains bound to DNA in high salt conditions, but the molecular reason for this is only partially understood. Importantly, the Mcm2-7 double hexamer serves as the platform for replisome assembly (On et al. 2014). During this process a number of replication factors and two S-phase kinases bind to the double-hexamer, which allows extrusion of one DNA strand from each Mcm2-7 ring prior to

processive DNA unwinding (Ilves et al. 2010; Labib 2010; Heller et al. 2011; Labib 2011; Siddiqui et al. 2013). The details of how these complex reactions occur are not understood (Tanaka and Araki 2013), but it is clear that ATP hydrolysis is central for Mcm2-7 helicase activity and DNA unwinding (Bochman and Schwacha 2008). The purified Mcm2-7 hexamer hydrolyzes ATP at an intermediate rate (Vijayraghavan and Schwacha 2012; Fernandez-Cid et al. 2013), but when integrated in the replisome the ATPase activity of the helicase becomes strongly activated (Ilves et al. 2010). How Mcm2-7 ATP-hydrolysis is regulated and what ATPase activity the important Mcm2-7 double-hexamer has is not known. Interestingly, one of the S-phase kinases, Dbf4-Dependent-Kinase Cdc7 (DDK), interacts with Mcm2 and Mcm4 (Sheu and Stillman 2010; Ramer et al. 2013), and phosphorylates specifically the chromatin-bound Mcm2-7 double-hexamer, but not the non-chromatin-bound single-hexamer (Sheu and Stillman 2006; Francis et al. 2009), suggesting that DDK recognizes a specific structure in the double-hexamer.

In this study, we examined by EM the helicase loading reaction in the presence of ATP, revealing the basic architecture of a number of pre-RC assembly reaction intermediates, including the OCM, a newly identified ORC-Cdc6-Mcm2-7-Mcm2-7 (OCMM) complex and the final product, the Mcm2-7 double hexamer. Through a systematic mapping strategy that employs subunit fusions with the maltose binding protein (MBP), we established the detailed architecture of the Mcm2-7 double hexamer. These structural analyses, in combination with ATP-hydrolysis assays, suggest a general pathway for pre-RC assembly, Mcm2-7 double hexamer stability on DNA during G1, mechanisms for blocking helicase activation within the Mcm2-7 double-hexamer and reveal a multi-hexamer binding site in the double hexamer for recruitment of the activating kinase DDK.

RESULTS

EM structure of the ORC-Cdc6-Mcm2-7 (OCM) complex

Reactions containing ORC-Cdc6, Cdt1-Mcm2-7 and DNA result in recruitment of the proteins to DNA, as measured by co-precipitation of the protein with DNA bound to beads after washing in low salt. The topological loading of the Mcm2-7 double-hexamer around the dsDNA was determined by washing the bead-bound DNA with high salt and under conditions that only the Mcm2-7 double hexamer remained DNA bound (Evrin et al. 2009; Remus et al. 2009). A trapped OCCM complex was obtained in the absence of ATP hydrolysis, but when ATP hydrolysis was allowed, Cdt1 was rapidly released from the OCCM and formation of an ORC-Cdc6-Mcm2-7 complex (OCM) occurred, which serves as the platform for Mcm2-7 double-hexamer assembly (Fernandez-Cid et al. 2013).

To study ATP-hydrolysis-dependent intermediates in the assembly reactions while the reaction transitioned from the OCCM to the double-hexamer, we harvested reaction products in the presence of 3 mM ATP at 2, 7, and 30 min time points, cross-linked them with glutaraldehyde, and then examined the samples by EM. Image classification of the spread complexes was used to analyze the products of the reaction. In addition to the expected fully assembled Mcm2-7 double-hexamer (DH) with a distinct, four-tiered side view (see below), we found two additional complexes, one of which was the expected three-tiered OCM complex (**Figure 1B**, lower panel), and the other was a new, five-tiered OCMM that will be described below. We found that in the 2-min sample the OCM particles dominated (96%), with a small percentage of OCMM particles (4%) and without observable DH. In the 30-min sample the DH particles dominated (99%), with an occasional OCMM particle (< 1%). In the 7-min sample, all three types of particles were present in significant numbers (**Table 1**): ~15% were OCM, ~10%

OCMM, and ~75% fully assembled double hexamers. We note that the high stability of Mcm2-7 double-hexamer may have inflated its observed frequency (Remus et al. 2009); it is therefore quite likely that the OCM and OCMM are more abundant than the ratio suggests at these time points during pre-RC formation.

The OCM was visualized by both negative stain EM and cryo-EM (**Figure 1B**). Compared to the 2D averages of the OCCM complex formed in the presence of ATP- γ S (**Figure 1B**, upper panel), the OCM particles were missing the distinct Cdt1 density located at the side of the Mcm2-7 hexamer (**Figure 1B**, lower panel). The OCCM structure was not observed in reactions that contained ATP instead of ATP γ S, highlighting that the OCCM is extremely short-lived. Interestingly, in the OCM, ORC-Cdc6 and Mcm2-7 appear to be more closely engaged than within the OCCM, which could reflect a functional difference, as the OCM, in contrast to the OCCM, is competent for Mcm2-7 double-hexamer formation.

The OCMM – a helicase loading intermediate containing an OCM and a second Mcm2-7 single hexamer

We found by negative stain EM a five-tiered structure, which we called OCMM, because it is comprised of one OCM and a second Mcm2-7 single hexamer (**Figure 2A**). In the four reference-free class averages of OCMM particles, the two Mcm2-7 hexamers were similar in structure to the fully assembly and isolated double-hexamer (**Figure 2B**). However, the left capping density is less well defined so we were uncertain whether Cdc6 remained associated with ORC at this stage. We assumed that Cdc6 was present because ORC was capable of repeated loading of the Mcm2-7 hexamer *in vitro* and the loading reaction required Cdc6 (Chen et al. 2007). The OCMM particles can also be observed in the pre-RC reaction without cross linking, although at much lower frequency (**Figure 2C**), suggesting that OCMM is a true pre-RC

intermediate. The fact that OCMM nearly peaks at 7 min and disappears at 30 min reaction time point indicates that it is a pre-RC assembly intermediate (**Table 1, Figure 2D**). The OCMM is likely a late stage intermediate because the two Mcm2-7 hexamers appear to have fully assembled into a double-hexamer (Tsakraklides and Bell 2010). Additional short-lived intermediates preceding the OCMM, such as a double OCM could exist, but we have not observed them among many thousands of molecules.

3D reconstruction of the Mcm2-7 double hexamer

Unlike the above-described OCM and OCMM that are transient and unstable helicase loading structures, the Mcm2-7 double hexamer is highly stable, which allows a more detailed analysis of the structure. The double hexamers were visible on a 3000-base pair circular plasmid when vitrified in the *in vitro* loading buffer and imaged by cryo-EM (**Supplementary figures 1A-C**). We selected several dozen of the double hexamer particles on plasmids and subjected them to image classification. The EM images demonstrated that the protein complexes that remained on the high-salt washed plasmid DNA were individual double-hexamers, and that the double-hexamers did not further interact to form higher order oligomers. The EM images further showed that dsDNA entered into the Mcm2-7 double-hexamer from one end of the long axis and exited from other, consistent with the notion that dsDNA passed through the central channel of the double hexamer (Evrin et al. 2009; Remus et al. 2009). The concentration of the plasmid-bound Mcm2-7 double-hexamer was too low for efficient EM data collection. To improve the sample yield and concentration, we assembled pre-RC complexes on biotinylated origin DNA linked to streptavidin-tagged magnetic beads, then washed the complexes with high salt and finally released the protein complex from the magnetic beads with DNase I and concentrated the sample. The double-hexamer particles had good contrast in the negatively stained raw EM

images and resulted in well-defined class averages, allowing a 3D EM reconstruction at 2-nm resolution (**Supplementary figures 1D-G, supplementary movie 1**). The 3D map reveals that the Mcm2-7 double-hexamer has an approximately cylindrical structure that is 21.5-nm long and 14-nm wide, with the two hexamers in the Mcm2-7 double hexamer slightly offset from the cylindrical axis and twisted relative to each other, similar to a previous EM structure (Remus et al. 2009). However, only in the current structure were individual protein subunits resolved, which allowed for a more detailed analysis.

Mapping the architecture of Mcm2-7 double hexamer

The identification of individual subunits in a 3D EM structure of a multi-protein complex allows for better understanding and interpretation of the data. Therefore we employed a 3D mapping strategy employing maltose binding protein (MBP) insertions into the N- or C-terminal region of individual MCM protein subunits similar to the strategy used for the OCCM (Sun et al. 2013), and assembled the MBP-inserted Mcm2-7 double hexamers one at a time (**Supplementary Figure 2**; asterisks). We found that Mcm2-7 hexamers with MBP insertion into either the N-terminal region of Mcm2, Mcm3, Mcm6, or Mcm7, or the C-terminal region of Mcm2 and Mcm5 could be properly loaded by ORC-Cdc6 and Cdt1 into double-hexamers, as shown by the reference-free class-averaged EM images (**Figure 3A**). The 3D reconstruction of each MBP-insertion double-hexamer clearly showed two extra densities compared to the wild type that could be unambiguously assigned to the inserted MBP (**Figure 3B**).

Each Mcm protein has two main domains, an N-terminal zinc-binding domain (NTD) and a C-terminal domain (CTD) that contains the AAA+ ATPase motifs. The eukaryotic Mcm subunits, Mcm2, Mcm4 and Mcm6 also have serine and threonine-rich, non-structured extensions on their very N-termini (NSD) that are targets for regulation by Cyclin-Dependent

Kinase (CDK), DDK and checkpoint kinase Mec1 (Randell et al. 2010; Tanaka and Araki 2013). Note that archaeal MCMs have both the NTD and CTD, but lack any amino-terminal extensions like the eukaryotic NSDs. Because the order of the subunits within the Mcm2-7 hexamer has been well established as Mcm5, 3, 7, 4, 6, 2 (Bochman et al. 2008; Costa et al. 2011; Lyubimov et al. 2012; Vijayraghavan and Schwacha 2012; Sun et al. 2013), mapping one Mcm protein would have been sufficient for assigning the remaining five MCM proteins if the handedness of the EM structure was determined, and mapping two Mcm proteins was sufficient to assign both the handedness and the identity for all proteins. We experimentally mapped the NTD of four Mcm protein subunits, more than sufficient to identify all NTDs as well as the handedness of the structure (**Figure 3B and 3C**). Unambiguous assignment for the identities of the six CTDs was facilitated by that fact that the CTDs should follow the same order of subunit arrangement and by our localization of the CTDs of Mcm2 and Mcm5 (**Figure 3B and 3D**). This completes the assignment of both the NTDs and CTDs for all Mcm protein subunits in the double-hexamer. If we consider the longitudinal axis of the double hexamer as the path of the DNA (i.e., vertical in the front and side views in **Figure 3B**), then the Mcm5 CTD in the upper hexamer was tilted $\sim 30^\circ$ towards right relative to the Mcm5 NTD. Indeed, a notable feature of all of the Mcm subunits in the double-hexamer is the staggered arrangement of the NTD ring relative to the CTD ring within a single Mcm2-7 complex in the double hexamer (**Figure 3D and Figure 4**). This is in stark contrast to the relative arrangement in the single Mcm2-7 hexamer and the CMG helicase, where the NTD and CTD rings are vertically aligned (Sun et al. 2013; Costa et al. 2014) (see discussion).

Segmentation and subunit assignment of the 3D EM map of Mcm2-7 double hexamer

We carried out semi-automatic density segmentation in Chimera (Pettersen et al. 2004).

First, the double hexamer was separated at the middle into two hexamers. Then, within each hexamer, six NTD densities were located in the middle of the double-hexamer and six CTD densities were located on the top and bottom of the double-hexamer. Finally, the NTDs and CTDs belonging to the same proteins as described above were merged and their subunit identities were assigned (**Figures 4A-4C**). The extra density near the center of the CTD ring is directly connected to the Mcm3 CTD and was therefore assigned as the Mcm3 C-terminal extension (3CTE; **Figures 4A and 4B**). The Mcm3 CTE was shown to activate the ATPase activities of ORC-Cdc6 (Frigola et al. 2013). The Mcm3 CTE partially protrudes from the end of the MCM hexamer, providing a structural basis for its function in the initial binding to ORC-Cdc6 (Frigola et al. 2013; Sun et al. 2013). Furthermore, its prominent position suggested that it could alter Mcm2-7 subunit interactions or influence Mcm2-7 ATP-hydrolysis. Indeed, we observed for Mcm2-7- Δ C3 in comparison to wild type (wt) Mcm2-7 reduced ATP hydrolysis activity that was even more reduced in the presence of Cdt1 (**Supplementary Figure 3**).

From the segmented and subunit-assigned structure, it is clear that the two-fold axis of the double-hexamer relating the two hexamers is a horizontal line running between subunits Mcm3, 7 at one side, and Mcm 2, 6 on the other side (**Figure 4A, Supplementary Movie 2**). Therefore, in the Mcm2-7 double hexamer, the NTDs of Mcm5, 3, 7, 4, 6, and 2 of one hexamer comes in to close proximity to the NTD of Mcm7, 3, 5, 2, 6, and 4 of the opposing hexamer, respectively. This arrangement places the NTD of both Mcm3 subunits adjacent to each other, but because the hexamers are in a head-to-head arrangement, the remaining subunits are opposite non-identical NTDs. For example, Mcm4 and Mcm6 that are adjacent on one hexamer associate with Mcm2 on the other, forming a composite hetero-trimer of Mcm2, Mcm4 and Mcm6. One prominent feature of the double-hexamer is that the NTD of several Mcm subunits protrudes

towards the CTD (**Figure 4A**, front view). This is most obvious in the case of Mcm4 and Mcm6, which have, in contrast to Mcm3 and Mcm5, long N-terminal extensions containing N-terminal serine and threonine rich, unstructured domains (NSD). Indeed the NSD of Mcm4 contains sequences that block the initiation of DNA replication until it is hyper-phosphorylated by the DDK kinase (**Supplementary Figure 2**) (Sheu and Stillman 2006; Sheu and Stillman 2010).

The two Mcm2 NTDs in the double-hexamer are related by the 2-fold axis and in close proximity to each other, whereas the neighboring Mcm6 NTD is situated up towards the CTD by 15 Å, and the next subunit, the Mcm4 NTD is situated further upwards of the Mcm6 NTD by yet another 15 Å, making the NTDs of Mcm2, Mcm6 and Mcm4 subunits form a staircase-like structure, as outlined by two blue lines (**Figure 4A**, back view, NTD's marked by red asterisks). Such an NTD arrangement occurs only at the backside of the double hexamer. On the front side, the NTDs of 3, 5, 7 are approximately co-planar (**Figure 4A**, front view). Thus, our analysis details how the individual Mcm-2-7 hexamers are twisted relative to each other.

The N-terminal domain (NTD) of *M. thermoautotrophicum* archaeal MCM that corresponds to the NTD of the eukaryotic MCM subunit had been crystallized in the double-hexameric form (Fletcher et al. 2003). This structure can be docked into the NTD rings of the 3D reconstruction of Mcm2-7 double hexamer (**Supplementary Figure 4A and 4C**). If we align the NTD of the nearly full-length archaeon *S. solfataricus* monomeric MCM crystal structure to an NTD of the docked archaeal NTD hexamer (Brewster et al. 2008), the C-terminal domain (CT) of the monomeric archaeal MCM falls into the CTD density of the segmented MCM subunits in the double-hexamer EM structure. The six Mcm proteins segmented from the double-hexamer are of a similar size and shape (**Supplementary Figure 4D**). They all have a bifurcated NTD that is connected to a globular CTD via a constricted linker region and approximately fit

with the rigid body-docked monomeric *S. solfataricus* MCM protein structure (Brewster et al. 2008). Notable differences exist, mainly in the top C-terminal region and the bottom N-terminal region where some of the eukaryotic Mcm subunits have evolved C-terminal extensions (CTE) and N-terminal extensions (NTE) of variable length (**Supplementary Figure 2**) (Vijayraghavan and Schwacha 2012). Another source of difference arises from the single rigid-body docking of the archaeal crystal structure, because the relative angle and position of NTD and CTD may be slightly different in the eukaryotic Mcm proteins. A movie of the double-hexamer structure docked with the *S. solfataricus* MCM crystal structure (in top hexamer) and the *M. thermoautotrophicum* NTD hexamer crystal structure (in bottom hexamer) is shown in **Supplementary Movie 3**.

The ATP hydrolysis activity of Mcm2-7 is inhibited in the double hexamer structure

The purified Mcm2-7 hexamer can hydrolyze ATP *in vitro* (Schwacha and Bell 2001; Ilves et al. 2010; Fernandez-Cid et al. 2013), but the active form of the helicase, when Mcm2-7 is part of a Cdc45-Mcm2-7-GINS (CMG) complex, has a significantly higher ATPase activity (Ilves et al. 2010). On the other hand, the ATPase rate of the Mcm2-7 double-hexamer is not known. The ~2 nm staggered and ~5° tilted stacking of the two hexamers, and the ~30° tilted arrangement of the individual Mcm proteins in the double hexamer as revealed by our EM study suggested that Mcm2-7 ATP hydrolysis could be altered (**Figure 5A**). We measured the ATP hydrolysis rate of the hexameric and double hexameric Mcm2-7 employing radioactive labeled ATP and found the ATP hydrolysis rate of the purified Mcm2-7 hexamer was 10.04 ± 0.66 pmol/min, similar to that previously observed (Schwacha and Bell 2001; Fernandez-Cid et al. 2013). In contrast, the *in vitro* assembled and purified Mcm2-7 double-hexamer had markedly reduced ATPase activity of 1.41 ± 0.02 pmol/min (**Figure 5B**). It is known that ATP is bound at

the interface between the Mcm subunits and that ATPase activity relies on accurate positioning of the catalytic residues in the Walker A and B motifs and the arginine finger of the adjacent AAA+ subunit (Davey et al. 2003; Bochman and Schwacha 2009; Wendler et al. 2012). We therefore suggest that the inhibition of the ATPase activity in the double hexamer is due to the tilted conformation of Mcm subunits, resulting in uncoupling of the ATP-hydrolysis motifs (**Figure 5A and 5C**). The observed ATPase rate of the double-hexamer is two orders of magnitude lower than the rate of the active *Drosophila melanogaster* CMG helicase (Ilves et al. 2010). Another possibility could be that the double-hexamer conformation per se is not compatible with ATP-hydrolysis. However, an MCM double hexamer of the thermophilic archaeon *Methanobacterium thermoautotrophicum* displays robust ATPase and helicase activity (Chong et al. 2000). Therefore we suggest that the tilted subunit arrangement in the eukaryotic double-hexamer is a powerful mechanism to restrict Mcm2-7 helicase activity in G1 phase and in S-phase prior to helicase activation (Diffley 2001).

Function of the Mcm 2/5 gate in the Mcm2-7 double-hexamer

The opening of the Mcm2-7 ring is central to helicase loading onto DNA. Indeed a DNA entry gate between Mcm2 and Mcm5 has been identified that is essential for pre-RC formation (Bochman and Schwacha 2008; Samel et al. 2014). If Mcm2-7 double-hexamer loading is a concerted process, as suggested (Remus et al. 2009; Yardimci and Walter 2014), then DNA insertion into both Mcm2-7 hexamers needs to be coordinated, requiring the Mcm2/5 gate of each hexamer to be aligned to promote simultaneous ring opening. However, the Mcm2-7 double-hexamer structure clearly shows that both Mcm2-7 rings are misaligned relative to the Mcm2/5 gate (**Figure 5D**). Thus our data show that Mcm2-7 loading must occur prior to double-hexamer formation, consistent with the finding that a single Mcm2-7 hexamer is loaded onto

DNA during OCCM formation, although the first hexamer requires ORC-Cdc6 for stability (Sun et al. 2013; Samel et al. 2014). The Mcm2-7 double-hexamer encircles dsDNA (Evrin et al. 2009; Remus et al. 2009), but the active helicase as part of the CMG encircles ssDNA (Fu et al. 2011), indicating that CMG formation in S phase involves remodeling of Mcm2-7 from a dsDNA to an ssDNA binding mode. This remodeling may involve opening of a gate between Mcm2 and Mcm5 (Bochman and Schwacha 2010; Costa et al. 2011; Samel et al. 2014). However, interactions between Mcm4 of one hexamer with Mcm2 and Mcm5 of the other hexamer may lock the complex in the closed conformation (**Figure 5D** and **5E**). Thus separation of both hexamers would have to precede or coincide with Mcm2-7 ring opening during helicase activation. In summary, we propose that the locked Mcm2/5 gate in the double-hexamer represents a fundamental mechanism to restrict Mcm2-7 ring opening and premature helicase activation, causing stability of the loaded double hexamer during G1 phase and until the initiation of DNA replication at that origin (Diffley 2001).

The Mcm2-7 double hexamer architecture provides a structural basis for it being a DDK target

DDK acts on the Mcm2-7 double hexamer, but not the single Mcm2-7 hexamer in solution and *in vivo* (Sheu and Stillman 2006; Randell et al. 2010; Heller et al. 2011; Ramer et al. 2013; Tanaka and Araki 2013), and the DDK action precedes the S-CDK action to activate the steps toward the actual initiation of DNA synthesis at each origin (Heller et al. 2011). However, it was unclear how DDK distinguishes a double hexamer from the single hexamer, as they both contain the same protein components. Recent studies found that DDK interacts with the NTDs of Mcm2 and Mcm4 (Sheu and Stillman 2010; Ramer et al. 2013). The architecture of the Mcm2-7 double hexamer as determined in the current study now provides a physical explanation to the

timed DDK action. Mcm2 and Mcm4 are far apart in the Mcm2-7 hexamer, separated by Mcm6. In the double hexamer, however, the NTD of Mcm2 and Mcm4 are in direct proximity, forming an integrated docking platform for the DDK (**Figure 5F**). Consistent with that, we found that the purified double hexamer is a far better substrate of DDK than the single hexamer *in vitro* (**Figure 5G**). Adjacent to the DDK docking domains in the Mcm2 and Mcm4 NTDs are the respective N-terminal, serine threonine rich unstructured domains (NSD) of each subunit that are the targets for DDK phosphorylation (Lei et al. 1997; Sheu and Stillman 2006; Sheu and Stillman 2010). Phosphorylation of the Mcm4 NSD is most critical since deletion of this intrinsic inhibitor of the initiation of DNA replication in Mcm2-7 bypasses the requirement for DDK (Sheu and Stillman 2010). Another mutation, *mcm5-bob1* (P83L) in the amino-terminus of the Mcm5 subunit also bypasses the requirement for DDK (Hardy et al. 1997). Interestingly, this amino acid lies adjacent to the Mcm4 and Mcm2 DDK docking domains (**Figure 5F**). The purified *bob-1* containing mutant double hexamer was unstable, but the DDK modified wild type double hexamer (**Supplementary figure 5A**) was stable and amenable to structural analysis. EM revealed that DDK modification neither separates the two hexamers nor drastically alters the overall structure of the double hexamer (**Supplementary figure 5B**) (On et al. 2014). Therefore, we suggest that phosphorylation mainly affects the surface properties of the double hexamer, to promote recruitment of additional helicase subunits such as GINS and Cdc45 and eventually Mcm2/5 gate opening and DNA unwinding (Labib 2010; On et al. 2014).

DISCUSSION

For a long time, eukaryotic replication licensing and pre-RC formation were merely abstract notions. Recent establishment of an *in vitro* helicase loading reaction with purified

proteins and origin DNA has transformed these concepts into tangible biochemical processes that are amenable to mechanistic dissections (Evrin et al. 2009; Remus et al. 2009; Mehanna and Diffley 2012). By taking advantage of the established *in vitro* pre-RC assembly process and the fact that the proteins form large complexes on DNA, we have succeeded in capturing and visualizing a number of pre-RC assembly steps by EM, which combined with image classification and detailed subunit mapping provided mechanistic insights into key eukaryotic replication initiation events (**Figure 6**, steps 1 - 7).

The role of the OCM in recruiting the second Mcm2-7 hexamer

The wild type OCM is a transient and salt sensitive pre-RC intermediate (Fernandez-Cid et al. 2013). It is therefore not feasible to obtain homogeneous OCM preparations for 3D reconstruction. Because we know the 3D EM structures of ORC-Cdc6 and the OCCM complexes (Sun et al. 2012; Sun et al. 2013), we are able to interpret the 2D structure of the OCM with confidence.

We know that the OCM is competent to recruit a second Mcm2-7 hexamer (Fernandez-Cid et al. 2013). The key question has been which part of the OCM structure is responsible for recruiting the next Cdt1-bound Mcm2-7 (Yardimci and Walter 2014). Our discovery that the interfaces between ORC-Cdc6 and Mcm2-7 in OCM and OCCM are similar is significant, as it indicates that the N-terminal surface of ORC-Cdc6 used for recruiting the first Mcm2-7 in OCCM remains shielded by the first hexamer in OCM, thus is not available for binding to the second Mcm2-7. It is also unlikely that ORC-Cdc6 could utilize the exposed C-terminal face to interact with a second Mcm2-7, because we have never observed in the EM images one ORC-Cdc6 sandwiched between two Mcm2-7 hexamers. We therefore suggest that the NTD section of the first loaded Mcm2-7 may have undergone conformational changes that allow direct

interaction with a second Mcm2-7 hexamer (**Figure 6**, step 4).

The implication of the OCMM structure in Pre-RC assembly

In the 7-min reaction sample, ~10% of pre-RC intermediates are OCMM particles (**Table 1**).

This is the first time the complex has been seen. Although Cdc6 is known to leave the origin at some point, we do not know if it leaves before the double hexamer assembly. In other words, we are uncertain if Cdc6 is actually present as the term OCMM implies. The OCMM could be formed by interaction of two OCM complexes followed by release of ORC/Cdc6. Alternatively, the OCM may be competent to recruit the second Mcm2-7 hexamer (**Figure 2D**), which would directly produce the OCMM complex as a Mcm2-7 double-hexamer precursor (**Figure 6**, step 4).

If so, why is the Mcm3 C terminus of the second hexamer, expected to be at the end of the double hexamer opposite to where ORC-Cdc6 binds, important for double hexamer assembly (Frigola et al. 2013)? The Mcm3 C-terminus influences not only the ATPase activity of ORC-Cdc6 (Frigola et al. 2013), but also the ATPase activity of the Mcm2-7 hexamer (**Supplementary Figure 3**), it appears possible that the Mcm3 C-terminus allosterically regulates the ATPase activity of the first loaded Mcm2-7 hexamer as well as that of the second hexamer yet to be loaded. Since Mcm2-7 ATPase is required for double hexamer assembly (Coster et al. 2014; Kang et al. 2014), the potential allosteric function may regulate double hexamer assembly.

The Mcm2-7 double-hexamer has tilted structure

One novel finding from our double-hexamer structure is that the Mcm proteins within each hexamer are tilted towards the right by nearly 30°, making the structure twisted and appearing to be spring loaded (**Figures 5A**). Discovery of the right-handed tilt was made possible due to our ability to unambiguously identify individual Mcm proteins and their respective N-terminal and C-terminal domains via the MBP insertion strategy. The twisted

feature appears to be unique to the eukaryotic double-hexamer. In the archaeal MCM hexamer structure modeled on a 3D EM map of the archaeal double-hexamer, which is an active helicase, the individual MCM proteins are arranged nearly parallel to the long cylindrical axis (Brewster et al. 2008). Furthermore, the Mcm proteins in both the yeast OCCM structure and the *Drosophila* Cdc45-Mcm2-7-GINS (CMG) helicase are not obviously twisted (Costa et al. 2011; Sun et al. 2013; Costa et al. 2014). Therefore, this twist in the Mcm2-7 proteins is specifically introduced during double-hexamer assembly and is relaxed in the active helicase (**Figure 6**, steps 5 and 6). We suggest that the twisting promotes long-term stability of the double hexamer on the DNA, as required for a molecule that licenses DNA replication in G1 phase for initiation of DNA replication at an origin much later in S phase.

Multiple mechanism inhibit the helicase activity in the Mcm2-7 double-hexamer

Helicase loading in bacteria and eukaryotes potentially involves similar mechanisms (Arias-Palomo et al. 2013; Sun et al. 2013), but results in very different complexes. In bacteria and eukaryotic viruses such as SV40 T Antigen and papillomavirus E1, the helicase is loaded in an active form, thus initiation is controlled at the level of initial DNA unwinding (Schuck and Stenlund 2005; Skarstad and Katayama 2013). In eukaryotes helicase loading cumulates in Mcm2-7 double-hexamer formation, which represents an intrinsically inactive form of the replicative helicase, which only becomes activated during S-phase (Tanaka and Araki 2013). If the helicase could be auto-activated and DNA polymerases would associate with the helicase, as happens in the case of the bacterial helicase, then helicase loading and helicase activation could occur simultaneously, resulting in re-replication and genome instability. In bacteria this cannot happen, as helicase loading becomes inhibited due to highly regulated DNA unwinding and helicase loading. In eukaryotes it is imperative that the Mcm2-7 double-hexamer by itself is

inactive as a helicase and only becomes activated after DNA licensing activity has been turned off. Multiple mechanisms control helicase loading during the G1-S transition, which have been studied extensively (Arias and Walter 2007; Siddiqui et al. 2013). In contrast, how premature helicase activation in G1 phase is regulated is only partially understood. Here we report two mechanisms that limit helicase activity of the Mcm2-7 double-hexamers. First, we observed that the Mcm2-7 subunits are arranged in an unusually tilted conformation and that the complex has in comparison to the Mcm2-7 single hexamer reduced ATPase activity, estimated to be two orders of magnitude lower than the ATPase of the active CMG helicase (Ilves et al. 2010). We suggest that the conserved Walker B motif in one subunit and the arginine-finger motif of a neighboring subunit, which together coordinate Mcm ATP hydrolysis, are misaligned in the Mcm2-7 double-hexamer (**Figure 5C**). Interestingly, within the OCCM and the *Drosophila* CMG helicase, the Mcm subunits are not tilted (Costa et al. 2011; Sun et al. 2013). Thus it appears possible that Orc1/Cdc6 ATP-hydrolysis could facilitate this structural change in Mcm2-7 during OCM formation (Fernandez-Cid et al. 2013), which also could be a prerequisite for Mcm2-7 hexamer dimerization (Evrin et al. 2014). A similar tilted conformation has to our knowledge not been observed in any AAA+ hexameric complex.

The second mechanism that regulates helicase activation involves the opening of the Mcm2-7 ring at a putative Mcm2/5 exit gate. Extrusion of one strand of the dsDNA is required to transform the Mcm2-7 double hexamer into an active helicase that encircles one ssDNA, while the other strand is extruded outside the center of the helicase. How the Mcm2-7 ring becomes opened during helicase activation is essentially unknown, but clearly Mcm2-7 ring opening at the Mcm2/5 gate would be very difficult, as the two Mcm2-7 rings are not aligned along the 2/5 axis. In summary, the Mcm2-7 helicase evolved from the bacterial helicase in multiple ways to

block premature helicase activation: the Mcm2-7 helicase is loaded on dsDNA (Evrin et al. 2009; Remus et al. 2009) and the inter-subunit interactions between each hexamer block the separation of the hexamers, the opening of the Mcm2-7 ring (**Figure 5D-E**) and strand extrusion, while the tilted subunit arrangement restricts the ATPase activity (**Figure 5A-C**).

It is known that DDK is essential for activation of the DNA helicase activity *in vivo* by recruitment of the GINS and Cdc45 (Siddiqui et al. 2013). The double hexamer structure shows the juxtaposition of Mcm2 and Mcm4 NTDs from opposing Mcm2-7 hexamers, creating a docking site for DDK (**Figure 5F**). This explains why DDK can only activate the Mcm2-7 hexamer that has been loaded onto DNA (**Figure 5**) and why Mcm4 NSD is phosphorylated only on Mcm4 subunits associated with chromatin (Sheu and Stillman 2010). Because DDK phosphorylation *per se* is insufficient to separate the double hexamer (On et al. 2014) (**Supplementary figure 5**), it is possible that phosphorylation promotes binding of additional factors including Cdc45 and GINS to untwist the double hexamer to produce two active helicases (**Figure 6**, step 6).

The twisted Mcm2-7 double-hexamer structure suggests a possible double stranded DNA melting mechanism

Because the dsDNA is known to be untwisted by the Mcm2-7 double-hexamer (Fu et al. 2011), we suggest that the right-hand twisted double-hexamer architecture may play a role in initial DNA melting. It is possible that when the double hexamer untwists itself as a result of DDK phosphorylation and binding of helicase activating factors (e.g, Cdc45 and GINS), it may unwind the dsDNA, causing the dsDNA to melt and the separated ssDNA to extrude from the central channel of the double-hexamer (**Figure 6**, step 6).

To summarize, we have captured and visualized by EM two new Mcm2-7 loading

intermediates (OCM and OCMM) in pre-RC assembly and established the detailed architecture of the Mcm2-7 double-hexamer, which identified key mechanism that inhibits the Mcm2-7 helicase activity in G1 phase. The structure of the double hexamer also explains how recruitment of DDK is restricted to Mcm2-7 on DNA *in vivo* as well as *in vitro*. Combined with the previously reported OCCM architecture, the structures of the four helicase-loading steps have improved our understanding of the multistep pre-RC assembly and will guide future biochemical and structural studies on DNA licensing and helicase activation.

MATERIALS AND METHODS

Expression and purification of proteins

ORC was expressed by using baculovirus-infected cells and purified as described (Klemm et al. 1997). Cdc6 and Cdt1 were expressed in bacteria and purified as described (Speck et al. 2005; Evrin et al. 2009). Mcm2-7 and MBP-Mcm2-7 were expressed in *Saccharomyces cerevisiae* and purified as described (Evrin et al. 2009; Fernandez-Cid et al. 2013). DDK was expressed and purified as described (Evrin et al. 2014). Most MBP-Mcm2-7 constructs were described in (Evrin et al. 2013; Fernandez-Cid et al. 2013), with the exception of Mcm2-MBP. During its construction using site-directed mutagenesis a restriction site was inserted after aa 712 in Mcm2. MBP was amplified from pMAL-c2X (NEB) with primers incorporating flexible linkers (sequences available on request) and inserted in the restriction sites, generating pCS624 (pESC-LEU-Mcm2-MBP/Mcm7).

***In vitro* assembly of pre-RC intermediates**

The pre-RC intermediates were assembled in a one-step reaction: 40 nM ORC, 80 nM Cdc6, 40 nM Cdt1 and 40nM MCM2-7 in buffer A (50 mM HEPES-KOH pH 7.5, 100 mM KGlu, 10

mM MgAc, 50 mM ZnAc, 3 mM ATP or ATP γ S, 5 mM DTT, 0.1% Triton X-100 and 5% glycerol) were added to 6 nM pUC19-ARS1 plasmid beads at 24 °C (Evrin et al. 2009). To capture the pre-RC assembly intermediates in the presence of ATP the reaction was stopped at various time points ranging from 2 to 30 min. For poly acrylamide gel electrophoresis (PAGE) and silver staining analysis, beads were washed three times with buffer A plus 1 mM EDTA or buffer B (50mM HEPES–KOH pH 7.5, 1 mM EDTA, 500 mM NaCl, 5% glycerol, 0.1% Triton X-100 and 5mM DTT) before digestion with 1 U of DNase I in buffer A plus 5 mM CaCl₂ for 6 min at 24 °C. For electron microscopy analysis, the beads were washed one time with buffer C (50 mM HEPES-KOH (pH 7.5), 100 mM potassium acetate, 5 mM magnesium acetate, 5 mM CaCl₂) and eluted with 0.003 U DNase I in 10 μ l buffer C, which was followed by the addition of glutaraldehyde to a final concentration of 0.2% for 15 min at 4 °C.

ATPase assay

The ATPase assay was performed as described (Speck and Stillman 2007; Fernandez-Cid et al. 2013). We used 2.5 pmol of Cdt1 and wild type or mutant Mcm2-7, which were incubated for 30 min on ice in 12 μ l of ATPase buffer [25 mM Hepes, pH 7.6, 100 mM KGlu, 5 mM MgAc, 1 mM DTT, 1 mM EDTA, 1 mM EGTA, 0.1% (v/v) Triton X-100, 10% glycerol] containing 1 mM ATP. After the incubation, 5 μ Ci of [α -³²P] ATP (3000 Ci/mmol) was added and the reaction was started by moving the tubes from ice into a 24°C water bath. 2 μ l aliquots were collected at 15, 30, 45, and 60 min and stopped with 0.5 μ l of stop solution (2% SDS, 50 mM EDTA). 1 μ l of the samples were consequently spotted on TLC plates and developed.

For the double-hexamer analysis 12 pre-RC assay reactions were prepared as described with minor modifications (Evrin et al. 2013). A one-step reaction was used. For a single reaction 40 nM ORC, 80 nM Cdc6, 40 nM Cdt1, 40 nM Mcm2-7 in buffer A [50 mM Hepes-KOH pH

7.5, 100 mM KGlu, 10 mM MgAc, 50 μ M ZnAc, 3 mM ATP, 5 mM DTT, 0.1% NP40, and 5% Glycerol] were added to 6 nM linear pUC19-ARS1 DNA coupled to magnetic beads for 15 min at 24 °C. Beads were washed 2 times with buffer A containing 300 mM NaCl and rinsed once with ATPase buffer [25 mM Hepes, pH 7.6, 100 mM KGlu, 5mM MgAc, 1mM DTT, 0.1% (v/v) NP40, 5% glycerol] before digestion with 12 μ l DNase I (1U) in ATPase buffer plus 5 mM CaCl₂ and 1 mM ATP for 5 min at 24 °C. The amount of released Mcm2-7 double-hexamer was quantified by SDS-PAGE and densitometry. About 0.8 pmol of Mcm2-7 single or double hexamer were used in the assay. Error bars represent the standard deviation from at least three independent experiments.

***In vitro* DDK kinase assays**

The pre-RCs were formed and washed with low salt or high salt as described above. Then pre-RCs or purified Mcm2-7 were incubated in buffer P [for non-radioactive assays] (50 mM Hepes-KOH pH 7.5, 100 mM KGlu, 10 mM MgAc, 50 μ M ZnAc, 3 mM ATP, 5 mM DTT, 0.1% Triton X-100, and 5% Glycerol) or in buffer P+ [for ³²P containing assays] (50 mM Hepes-KOH pH 7.5, 100 mM KGlu, 10 mM MgAc, 50 μ M ZnAc, 0.1 mM ATP, 5 mM DTT, 0.1% Triton X-100, and 5% Glycerol, 100 μ Ci/ml γ -³²P ATP) containing 5-80 nM DDK (40 nM in case of figure 5G) and incubated at 27°C for 15 min. For EM analysis we used 80 nM DDK treated samples. After an additional wash with buffer A plus 5 mM CaCl₂ (for PAGE analysis) or buffer C (for EM analysis) the DNA was digested by 1 U of DNase I for 6 min at 24°C. Proteins were analyzed by EM or separated on a 7.5% SDS-polyacrylamide gel and silver stained. The incorporation of ³²P-phosphate was detected by autoradiography of the silver stained gel.

***In vitro* assembly and purification of the wild type and MBP-inserted Mcm2-7 double-hexamers for single particle EM**

The pre-RC were assembled in a one-step reaction: 40 nM ORC, 80 nM Cdc6, 40 nM Cdt1 and 40nM MCM2–7 or MBP-Mcm2-7 in buffer A (50 mM HEPES–KOH pH 7.5, 100 mM KGlu, 10mM MgAc, 50 mM ZnAc, 3 mM ATP, 5 mM DTT, 0.1% Triton X-100 and 5% glycerol) were added to 6 nM pUC19-ARS1 plasmid beads at 24 °C (Evrin et al. 2009). After 15 minutes the beads were washed three times with buffer B and three times with buffer C and eluted with 1 U DNase I in 5 µl buffer C. For the cryo-EM analysis 20 elutions were pooled and 10x concentrated with an Amicon concentrator (Ultracel 100K).

Electron microscopy

For negative stain EM, about 3 µl samples were deposited on the EM grids, after 60 s, the grids were blotted with a piece of filter paper, deposited a 4-µl drop of 1% uranyl acetate aqueous solution. After waiting for 30 s, the stain solution was blotted, and a second 4-µl drop of stain solution was deposited, and waited for 60 s, then blotted and left for air drying. To achieve ideal staining, we found it was important to leave a thin layer of stain solution on the grid during the last blotting, such that there was enough stain salt to fully embed the particles but not too much to make the grid too dark in EM. For cryo-EM of plasmid-bound double hexamer, we glow discharged the holey carbon grids coated with a thin continuous carbon film just before use, pipetted 3-µl sample on a EM grid, and waited for 1 min, before blotting for 5 s, and plunge-froze the grid into liquid ethane. Sample was vitrified in an FEI Vitrobot with sample chamber temperature set to 11 °C, relative humidity 70%, and blotting pad position offset -1 mm. We used the JEM-2010F to record images at a low electron dose of $15 \text{ e}^-/\text{\AA}^2$ at a magnification of 50,000x in a 4k x 4k Gatan Ultrascan CCD camera. The EM image sampling size corresponds to 2.12 Å/pixel at the specimen level. Negative stain EM was performed at room temperature and cryo-EM was done using a Gatan 626 cryo-specimen holder with the specimen temperature

maintained below -170 °C.

Single particle image analysis and 3D reconstruction

Individual particle images were manually selected on a computer display with the e2boxer in the EMAN2 package (Tang et al. 2007). The contrast transfer function (CTF) parameters were determined separately by ctfit in EMAN for all particles from each CCD frame. The particle images were phase flipped, high-pass filtered ($hp = 1$), normalized with the edgenorm option, and pooled into one image stack. We then carried out reference-free 2D image classification and averaging with refine2d.py. We found that binning the particle images by a factor of 2 and then low-pass filter to 20 Å produced best results. Particle selection of the Mcm2-7 loading intermediates in ATP relied on the fact that they are large protein complexes with the distinct parallel line feature in the side views. The manually selected particle images were subjected to multiple rounds of reference-free classification. The particle images belonging to classes that were not in the near perfect side views were removed.

For 3D reconstruction of the purified wild type Mcm2-7 double hexamer, a dataset of ~ 22,630 raw particle images was used. A 3D volume was calculated using the startcsym program with the C6 symmetry in EMAN, taking advantage of the pseudo 6-fold symmetry of the structure. The volume was first refined in the D6 symmetry and the resulting 3D volume was then low-pass filtered to 100 Å to minimize initial model bias, and the volume was rotated by 90° so the true 2-fold axis of the double hexamer was aligned to the Z-axis. This starting model is essentially a 3D blob with the correct size but without any structural features. The starting model was then refined by projection matching with the raw particle images in EMAN with the C2 symmetry and without amplitude correction. The final 3D map has a resolution of ~ 15 Å as estimated by the traditional Fourier shell correlation at 0.5 threshold, and ~ 20 Å as estimated by

the gold standard Fourier shell correlation at 0.143 threshold. The negative stain 3D EM density map of *S. cerevisiae* Mcm2-7 double-hexamer has been deposited in the Electron Microscopy Data Bank under accession code EMD-5857.

For the purified MBP-inserted Mcm2-7 double hexamer samples, the final negative stain EM dataset contained 5358, 9917, 8867, 8224, 1368, 28474 particle images for double hexamers with MBP insertion in the N-terminal region of Mcm2, Mcm3, Mcm6, Mcm7, and C-terminal region of Mcm2 and Mcm5, respectively. The raw images were processed similarly as the wild type double hexamer images. 3D refinement of the MBP-insertion double hexamers used the wild-type double hexamer 3D map as the starting model. We relaxed and optimized the mask size during refinement to avoid cutting off the protruding MBP densities while minimizing noise. The 3D maps of the MBP insertion double hexamers had a resolution ranging from 25 Å to 35 Å. The DDK-modified double hexamer dataset had 3063 raw particles and the 3D map had a resolution of 34 Å. EM map surface rendering, density segmentation, and docking with crystal structures were carried out in the UCSF chimera (Pettersen et al. 2004).

ACKNOWLEDGEMENTS

We acknowledge the help of Cecile Evrin and Stefan Samel in the early stages of this project. This work was supported by National Institutes of Health grant nos. GM45436 (to B.S.) and GM74985 (to H.L.) and the United Kingdom Medical Research Council (to C.S.). J.S., A.R. A.F. and S.T. performed the specimen preparation and biochemistry. J.S. and Z.Y. collected the EM data, performed the EM reconstructions. J.S., A.R., A.F., B.S., C.S., and H.L. designed experiments and wrote the manuscript.

REFERENCES

- Arias EE, Walter JC. 2007. Strength in numbers: preventing rereplication via multiple mechanisms in eukaryotic cells. *Genes Dev* 21: 497-518.
- Arias-Palomo E, O'Shea VL, Hood IV, Berger JM. 2013. The Bacterial DnaC Helicase Loader Is a DnaB Ring Breaker. *Cell* 153: 438-448.
- Bell SP, Dutta A. 2002. DNA replication in eukaryotic cells. *Annu Rev Biochem* 71: 333-374.
- Bell SP, Stillman B. 1992. ATP-dependent recognition of eukaryotic origins of DNA replication by a multiprotein complex. *Nature* 357: 128-134.
- Bochman ML, Bell SP, Schwacha A. 2008. Subunit organization of Mcm2-7 and the unequal role of active sites in ATP hydrolysis and viability. *Mol Cell Biol* 28: 5865-5873.
- Bochman ML, Schwacha A. 2008. The Mcm2-7 complex has in vitro helicase activity. *Mol Cell* 31: 287-293.
- . 2009. The Mcm complex: unwinding the mechanism of a replicative helicase. *Microbiol Mol Biol Rev* 73: 652-683.
- . 2010. The *Saccharomyces cerevisiae* Mcm6/2 and Mcm5/3 ATPase active sites contribute to the function of the putative Mcm2-7 'gate'. *Nucleic Acids Res* 38: 6078-6088.
- Brewster AS, Wang G, Yu X, Greenleaf WB, Carazo JM, Tjajadi M, Klein MG, Chen XS. 2008. Crystal structure of a near-full-length archaeal MCM: functional insights for an AAA+ hexameric helicase. *Proc Natl Acad Sci U S A* 105: 20191-20196.
- Chen S, de Vries MA, Bell SP. 2007. Orc6 is required for dynamic recruitment of Cdt1 during repeated Mcm2-7 loading. *Genes Dev* 21: 2897-2907.
- Chong JP, Hayashi MK, Simon MN, Xu RM, Stillman B. 2000. A double-hexamer archaeal minichromosome maintenance protein is an ATP-dependent DNA helicase. *Proc Natl Acad Sci U S A* 97: 1530-1535.
- Costa A, Ilves I, Tamberg N, Petojevic T, Nogales E, Botchan MR, Berger JM. 2011. The structural basis for MCM2-7 helicase activation by GINS and Cdc45. *Nat Struct Mol Biol* 18: 471-477.
- Costa A, Renault L, Swuec P, Petojevic T, Pesavento J, Ilves I, MacLellan-Gibson K, Fleck RA, Botchan MR, Berger JM. 2014. DNA binding polarity, dimerization, and ATPase ring remodeling in the CMG helicase of the eukaryotic replisome. *eLife*: e03273.
- Coster G, Frigola J, Beuron F, Morris EP, Diffley JF. 2014. Origin Licensing Requires ATP Binding and Hydrolysis by the MCM Replicative Helicase. *Mol Cell*.
- Davey MJ, Indiani C, O'Donnell M. 2003. Reconstitution of the Mcm2-7p heterohexamer, subunit arrangement, and ATP site architecture. *J Biol Chem* 278: 4491-4499.
- Diffley JF. 2001. DNA replication: building the perfect switch. *Curr Biol* 11: R367-370.
- Evrin C, Clarke P, Zech J, Lurz R, Sun J, Uhle S, Li H, Stillman B, Speck C. 2009. A double-hexameric MCM2-7 complex is loaded onto origin DNA during licensing of eukaryotic DNA replication. *Proc Natl Acad Sci U S A* 106: 20240-20245.
- Evrin C, Fernandez-Cid A, Riera A, Zech J, Clarke P, Herrera MC, Tognetti S, Lurz R, Speck C. 2014. The ORC/Cdc6/MCM2-7 complex facilitates MCM2-7 dimerization during prereplicative complex formation. *Nucleic Acids Res* 42: 2257-2269.
- Evrin C, Fernandez-Cid A, Zech J, Herrera MC, Riera A, Clarke P, Brill S, Lurz R, Speck C. 2013. In the absence of ATPase activity, pre-RC formation is blocked prior to MCM2-7 hexamer dimerization. *Nucleic Acids Res*.
- Fernandez-Cid A, Riera A, Tognetti S, Herrera MC, Samel S, Evrin C, Winkler C, Gardenal E, Uhle S, Speck C. 2013. An ORC/Cdc6/MCM2-7 Complex Is Formed in a Multistep Reaction to Serve as

- a Platform for MCM Double-Hexamer Assembly. *Mol Cell* **50**: 577-588.
- Fletcher RJ, Bishop BE, Leon RP, Sclafani RA, Ogata CM, Chen XS. 2003. The structure and function of MCM from archaeal *M. Thermoautotrophicum*. *Nat Struct Biol* **10**: 160-167.
- Francis LI, Randell JC, Takara TJ, Uchima L, Bell SP. 2009. Incorporation into the prereplicative complex activates the Mcm2-7 helicase for Cdc7-Dbf4 phosphorylation. *Genes Dev* **23**: 643-654.
- Frigola J, Remus D, Mehanna A, Diffley JF. 2013. ATPase-dependent quality control of DNA replication origin licensing. *Nature* **495**: 339-343.
- Fu YV, Yardimci H, Long DT, Ho TV, Guainazzi A, Bermudez VP, Hurwitz J, van Oijen A, Scharer OD, Walter JC. 2011. Selective bypass of a lagging strand roadblock by the eukaryotic replicative DNA helicase. *Cell* **146**: 931-941.
- Hardy CF, Dryga O, Seematter S, Pahl PM, Sclafani RA. 1997. mcm5/cdc46-bob1 bypasses the requirement for the S phase activator Cdc7p. *Proc Natl Acad Sci U S A* **94**: 3151-3155.
- Heller RC, Kang S, Lam WM, Chen S, Chan CS, Bell SP. 2011. Eukaryotic origin-dependent DNA replication in vitro reveals sequential action of DDK and S-CDK kinases. *Cell* **146**: 80-91.
- Ilves I, Petojevic T, Pesavento JJ, Botchan MR. 2010. Activation of the MCM2-7 helicase by association with Cdc45 and GINS proteins. *Mol Cell* **37**: 247-258.
- Kang S, Warner MD, Bell SP. 2014. Multiple Functions for Mcm2-7 ATPase Motifs during Replication Initiation. *Mol Cell*.
- Klemm RD, Austin RJ, Bell SP. 1997. Coordinate binding of ATP and origin DNA regulates the ATPase activity of the origin recognition complex. *Cell* **88**: 493-502.
- Labib K. 2010. How do Cdc7 and cyclin-dependent kinases trigger the initiation of chromosome replication in eukaryotic cells? *Genes Dev* **24**: 1208-1219.
- . 2011. Building a double hexamer of DNA helicase at eukaryotic replication origins. *Embo J* **30**: 4853-4855.
- Lei M, Kawasaki Y, Young MR, Kihara M, Sugino A, Tye BK. 1997. Mcm2 is a target of regulation by Cdc7-Dbf4 during the initiation of DNA synthesis. *Genes Dev* **11**: 3365-3374.
- Lyubimov AY, Costa A, Bleichert F, Botchan MR, Berger JM. 2012. ATP-dependent conformational dynamics underlie the functional asymmetry of the replicative helicase from a minimalist eukaryote. *Proc Natl Acad Sci U S A* **109**: 11999-12004.
- Mehanna A, Diffley JF. 2012. Pre-replicative complex assembly with purified proteins. *Methods* **57**: 222-226.
- On KF, Beuron F, Frith D, Snijders AP, Morris EP, Diffley JF. 2014. Prereplicative complexes assembled in vitro support origin-dependent and independent DNA replication. *EMBO J* **33**: 605-620.
- Pettersen EF, Goddard TD, Huang CC, Couch GS, Greenblatt DM, Meng EC, Ferrin TE. 2004. UCSF Chimera--a visualization system for exploratory research and analysis. *J Comput Chem* **25**: 1605-1612.
- Pospiech H, Grosse F, Pisani FM. 2010. The initiation step of eukaryotic DNA replication. *Subcell Biochem* **50**: 79-104.
- Ramer MD, Suman ES, Richter H, Stanger K, Spranger M, Bieberstein N, Duncker BP. 2013. Dbf4 and Cdc7 proteins promote DNA replication through interactions with distinct Mcm2-7 protein subunits. *J Biol Chem* **288**: 14926-14935.
- Randell JC, Bowers JL, Rodriguez HK, Bell SP. 2006. Sequential ATP hydrolysis by Cdc6 and ORC directs loading of the Mcm2-7 helicase. *Mol Cell* **21**: 29-39.
- Randell JC, Fan A, Chan C, Francis LI, Heller RC, Galani K, Bell SP. 2010. Mec1 is one of multiple

- kinases that prime the Mcm2-7 helicase for phosphorylation by Cdc7. *Mol Cell* **40**: 353-363.
- Remus D, Beuron F, Tolun G, Griffith JD, Morris EP, Diffley JF. 2009. Concerted loading of Mcm2-7 double hexamers around DNA during DNA replication origin licensing. *Cell* **139**: 719-730.
- Remus D, Diffley JF. 2009. Eukaryotic DNA replication control: lock and load, then fire. *Curr Opin Cell Biol* **21**: 771-777.
- Samel SA, Fernandez-Cid A, Sun J, Riera A, Tognetti S, Herrera MC, Li H, Speck C. 2014. A unique DNA entry gate serves for regulated loading of the eukaryotic replicative helicase MCM2-7 onto DNA. *Genes Dev* **28**: 1653-1666.
- Schuck S, Stenlund A. 2005. Assembly of a double hexameric helicase. *Mol Cell* **20**: 377-389.
- Schwacha A, Bell SP. 2001. Interactions between two catalytically distinct MCM subgroups are essential for coordinated ATP hydrolysis and DNA replication. *Mol Cell* **8**: 1093-1104.
- Sheu YJ, Stillman B. 2006. Cdc7-Dbf4 phosphorylates MCM proteins via a docking site-mediated mechanism to promote S phase progression. *Mol Cell* **24**: 101-113.
- . 2010. The Dbf4-Cdc7 kinase promotes S phase by alleviating an inhibitory activity in Mcm4. *Nature* **463**: 113-117.
- Siddiqui K, On KF, Diffley JF. 2013. Regulating DNA replication in eukarya. *Cold Spring Harbor perspectives in biology* **5**.
- Skarstad K, Katayama T. 2013. Regulating DNA replication in bacteria. *Cold Spring Harbor perspectives in biology* **5**: a012922.
- Speck C, Chen Z, Li H, Stillman B. 2005. ATPase-dependent cooperative binding of ORC and Cdc6 to origin DNA. *Nat Struct Mol Biol* **12**: 965-971.
- Speck C, Stillman B. 2007. Cdc6 ATPase activity regulates ORC x Cdc6 stability and the selection of specific DNA sequences as origins of DNA replication. *J Biol Chem* **282**: 11705-11714.
- Sun J, Evrin C, Samel SA, Fernandez-Cid A, Riera A, Kawakami H, Stillman B, Speck C, Li H. 2013. Cryo-EM structure of a helicase loading intermediate containing ORC-Cdc6-Cdt1-MCM2-7 bound to DNA. *Nat Struct Mol Biol* **20**: 944-951.
- Sun J, Kawakami H, Zech J, Speck C, Stillman B, Li H. 2012. Cdc6-induced conformational changes in ORC bound to origin DNA revealed by cryo-electron microscopy. *Structure* **20**: 534-544.
- Takara TJ, Bell SP. 2011. Multiple Cdt1 molecules act at each origin to load replication-competent Mcm2-7 helicases. *Embo J* **30**: 4885-4896.
- Tanaka S, Araki H. 2013. Helicase activation and establishment of replication forks at chromosomal origins of replication. *Cold Spring Harbor perspectives in biology* **5**.
- Tang G, Peng L, Baldwin PR, Mann DS, Jiang W, Rees I, Ludtke SJ. 2007. EMAN2: an extensible image processing suite for electron microscopy. *J Struct Biol* **157**: 38-46.
- Tsakraklides V, Bell SP. 2010. Dynamics of pre-replicative complex assembly. *J Biol Chem* **285**: 9437-9443.
- Vijayraghavan S, Schwacha A. 2012. The eukaryotic Mcm2-7 replicative helicase. *Subcell Biochem* **62**: 113-134.
- Wendler P, Ciniawsky S, Kock M, Kube S. 2012. Structure and function of the AAA+ nucleotide binding pocket. *Biochim Biophys Acta* **1823**: 2-14.
- Yardimci H, Walter JC. 2014. Prereplication-complex formation: a molecular double take? *Nat Struct Mol Biol* **21**: 20-25.

TABLE

Table 1. The observed particle numbers and percentages of the three pre-RC loading intermediates in the presence of 3 mM ATP. The OCM, OCCM, and the double-hexamer (DH) were found in >300 raw electron micrographs of negative stained and cross-linked samples at 2, 7, and 30 min of reaction time. Note that the 7-min reaction experiment was performed independently for two times.

Particle #, (%)	2 min (I)	7 min (I)	7 min (II)	30 min (I)
OCM	124 (96%)	171 (15%)	314 (17%)	0 (0%)
OCCM	5 (4%)	102 (9%)	192 (10%)	10 (0.8%)
DH	0 (0%)	866 (76%)	1349 (73%)	1259 (99.2%)

FIGURE LEGENDS

Figure 1. The multiple-step pre-RC assembly process and EM visualization of intermediates during recruitment of the first Mcm2-7 hexamer by ORC-Cdc6

(A) A sketch for loading of Mcm2-7 double hexamer highlighting three unresolved issues as shown by three question marks: (1) Does ATP hydrolysis and Cdt1 release from OCCM lead to a large gap between ORC-Cdc6 and Mcm2-7 that may allow ORC-Cdc6 to recruit a second Mcm2-7 hexamer (step 3)? (2) How is the second Mcm2-7 hexamer recruited (step 4)? (3) How are the two Mcm2-7 hexamers arranged in the double hexamer (step 5)?

(B) The OCM structure compared with the OCCM structure. Upper panel: 2D class averages of cryo-EM (upper row) and negative stain images (lower row) of OCCM formed in the presence of ATP- γ S. Red arrows point to the Cdt1 density identified previously. Lower panel: 2D class averages of OCM in the presence of ATP at 7 min reaction time by cryo-EM (upper row) and negative stain EM (lower row). Blue arrows point to the regions where Cdt1 is missing. In both panels, a selected 2D average is enlarged and overlaid with sketches of the proposed ORC-Cdc6

region in orange and the Mcm2-7 region in purple. Scale bar is 15 nm.

Figure 2. A novel loading intermediate containing one OCM and one Mcm2-7 hexamer

(A) Four class-averaged negative-stain EM images of the novel five-tiered Mcm2-7 loading intermediate. Particles were selected from sample that was incubated in 3 mM ATP for 7 min followed by 0.1% glutaraldehyde crosslinking.

(B) Selected reference-free 2D averages of Mcm2-7 double hexamer found in the same sample as (A).

(C) The OCMM raw particle images found in the 7 min reaction sample without glutaraldehyde crosslinking.

(D) The OCMM is an on-pathway intermediate during the loading of the Mcm2-7 double hexamer. The question mark (?) denotes possible existence of additional intermediate(s) upstream of OCMM.

Figure 3. 3D reconstructions of six MBP inserted Mcm2-7 double hexamers

(A) Two selected reference-free class averages of the double hexamer with MBP inserted to the N-terminal region of Mcm2 (MBP-M2); MBP-M3; MBP-M6; and MBP-M7, and MBP inserted to the C-terminal region of Mcm2 (M2-MBP) and M5-MBP. Blue asterisks mark the extra and peripheral MBP densities. Box size is 36 nm.

(B) Each column shows the top, front, and side views of the six MBP-fused Mcm2-7 double hexamers. The MBP density is colored blue in the 3D map. The bottom panels show horizontal sections of the 3D maps at the inserted MBP positions as indicated by dashed lines. Blue asterisks mark the MBP densities in the sections. Box size in the bottom panel is 24 nm.

(C) The Mcm subunit arrangement in the lower hexamer as viewed from the N-termini (left) and in the upper hexamer viewed from the C-termini (right).

(D) NTD and CTD assignment of each Mcm subunit in the top hexamer of the double hexamer as viewed from the side. The NTDs and the CTDs are staggered such that each Mcm subunit is tilted in the hexamer and the double hexamer is twisted. The Mcm protein domains labeled with red numbers in (C) and (D) are positively identified in this study, the domains in blue numbers are inferred from the known order of subunits in the hexamer.

Figure 4. The architecture of the Mcm2-7 double hexamer

(A) Four side views of the 3D map of the wild type Mcm2-7 double hexamer consecutively rotated 90° around a vertical axis. The six Mcm proteins are colored differently and labeled correspondingly. A pair of blue lines trace the helical arrangement of the NTDs (red asterisks) of Mcm2, 6, and 4 (back side view). The black ovals in the front and back views indicate the position of the 2-fold axis.

(B) Top and bottom views of the Mcm2-7 CTD ring. A density that is connected to CTD of Mcm3 and located near the hexamer center is tentatively assigned as the C-terminal extension of Mcm3 (3-CTE).

(C) Top and bottom views of the Mcm2-7 NTD ring. Overlapping the two views by translation generates the interface between two hexamers of the Mcm2-7 double hexamer. Mcm2-Mcm5 in one hexamer is approximately aligned with Mcm4-Mcm6 in the other.

Figure 5. Functional implications of the Mcm2-7 double hexamer structure

(A) There are two types of tilt found in the double hexamer EM structure. The first is the end-to-end stacking of the two hexamers that is staggered by ~ 2 nm, and tilted by ~ 5° off the vertical cylinder axis. The second is a ~ 30° tilt of individual Mcm subunits in each hexamer with respect to the vertical axis.

(B) The ATP hydrolysis rates were determined for the Mcm2-7 helicase in single and double

hexamer conformations. The single hexamer (H) exhibits a robust ATPase activity that is strongly reduced in the double hexamer configuration (DH).

(C) A speculative sketch illustrating that the arginine finger (R) of one Mcm subunit in the hexamer is properly positioned towards the Walker A and B motifs (A/B) of a neighbor protein for ATPase activity (left). Subunit tilt in the double hexamer misaligns the arginine finger (R) with respect to the A/B motifs and abolishes the ATPase activity (right).

(D) The backside view of the double hexamer structure shows that the Mcm2/5 interface in the upper hexamer is nearly opposite to the Mcm2/5 interface in the lower hexamer. The NTD of Mcm4 (M4N) wedges against the potential Mcm2/5 gate.

(E) A sketch illustrating that the potential Mcm2/5 is unconstrained in the single hexamer (left), but is constrained or locked by structural features such as Mcm4 NTD of the opposing hexamer in the double hexamer.

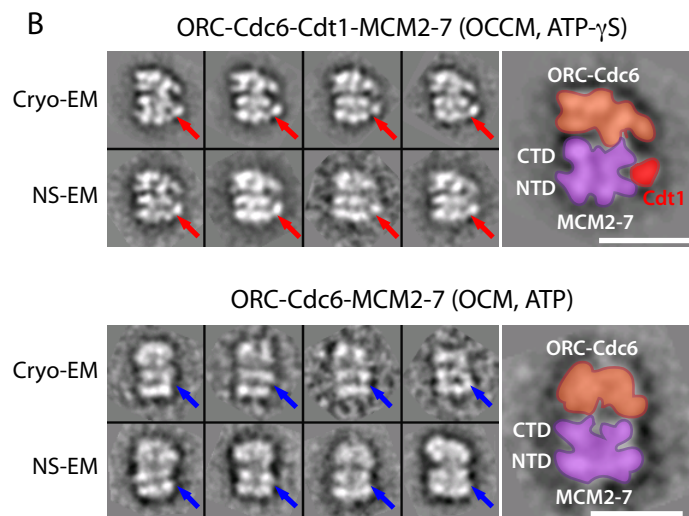
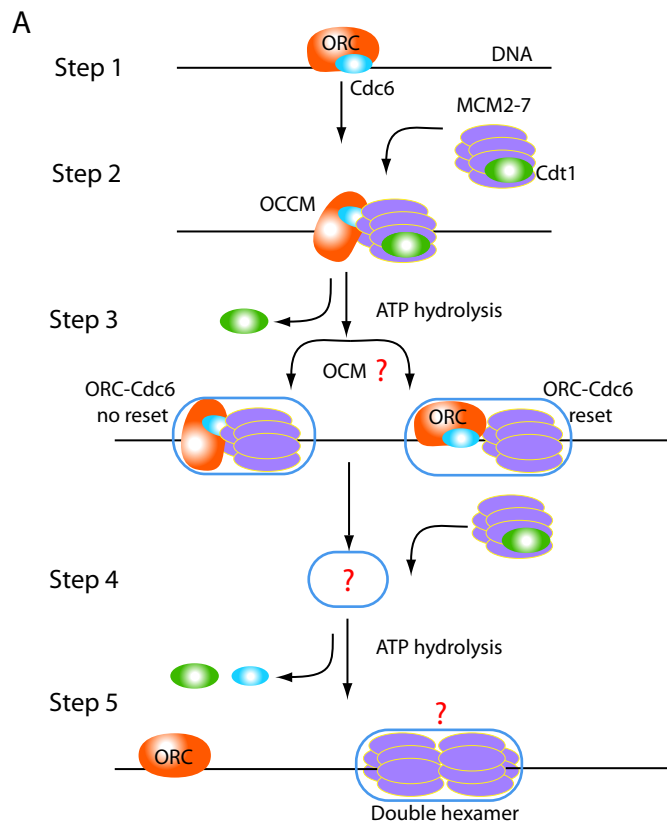
(F) A model for DDK interaction with the Mcm2-7 double hexamer, but not with the single hexamer. The heterodimeric DDK requires a bipartite binding site (NTDs of Mcm2 and Mcm4) that is not available in the single hexamer, but available in the double hexamer. The double hexamer is in the right side view as in Fig 4A.

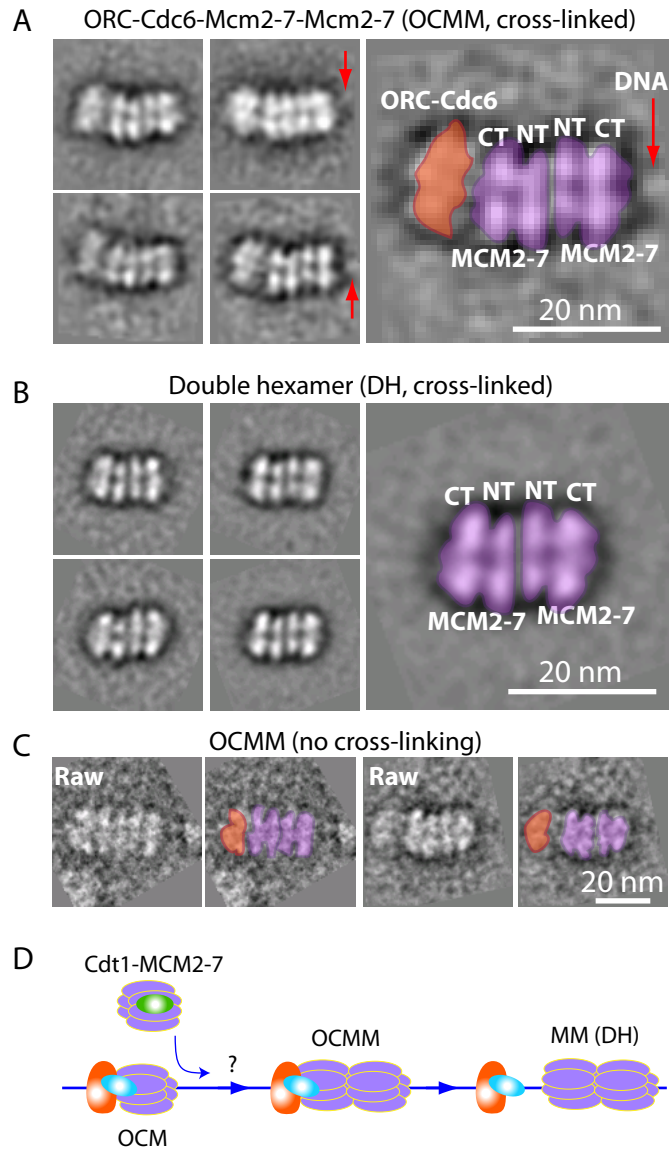
(G) DDK activity on the purified single versus double Mcm2-7 hexamers. Upper panels are by silver staining, and lower panel by ³²P autoradiography.

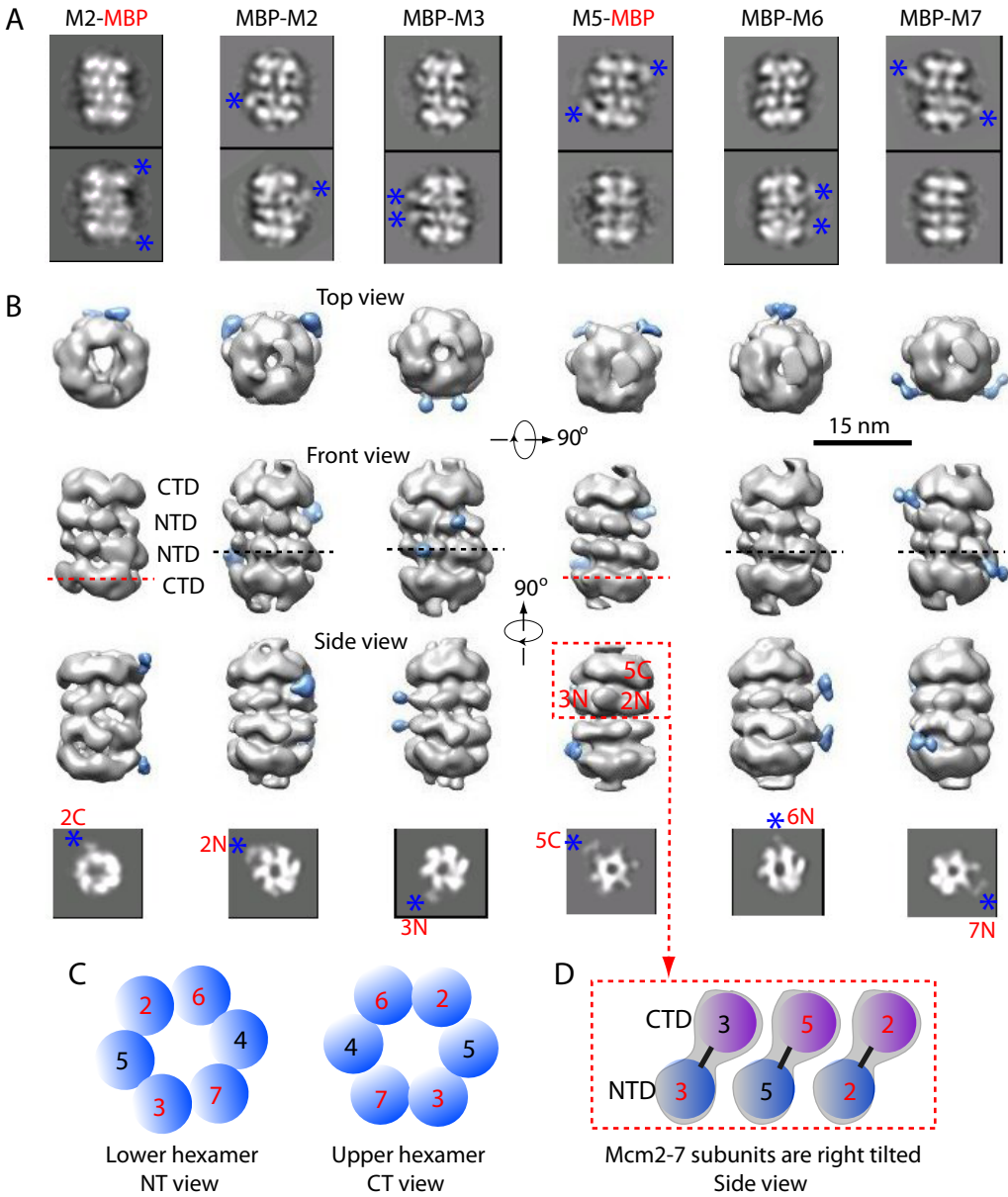
Figure 6. EM of Pre-RC intermediates suggests possible helicase loading and initial DNA melting mechanisms

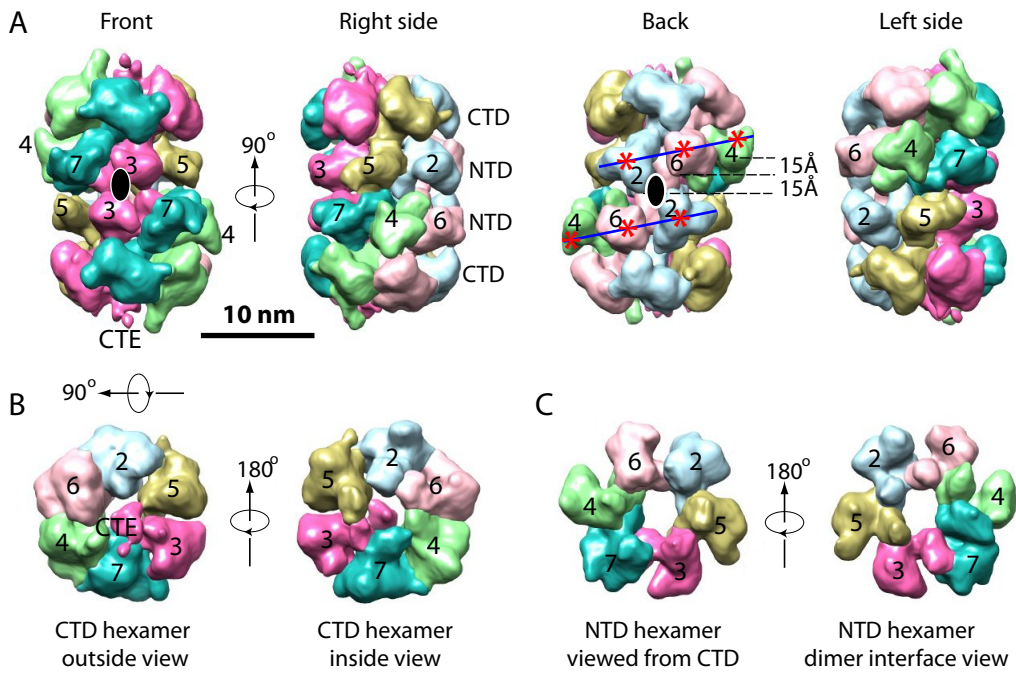
Steps 1 - 5 describe the proposed model for the eukaryotic pre-RC formation. Each of the five steps as drawn is based on an experimentally captured Mcm2-7 loading intermediate. ORC-Cdc6 on origin DNA in step 1 is the activated platform for loading of Cdt1-Mcm2-7. Formation of

OCCM shown in step 2 represents the recruitment of the first hexamer. ATP hydrolysis in step 3 leads to the release of Cdt1 and formation of OCM. Formation of the OCMM in step 4 completes of the recruitment of the second hexamer. The question mark in step 4 indicates a possible short-lived intermediate not captured in the current study. In step 5, ATP hydrolysis by ORC-Cdc6 leads to maturation of the double hexamer structure on DNA and its separation from ORC-Cdc6. Mcm subunits are colored purple in the single hexamer, but orange in the double hexamer to highlight the subunit tilt. The two hexamers in the OCMM are also colored orange (step 4), because their structure is highly similar to the final double hexamer. The OCM, OCMM, and double hexamer in steps 3, 4, and 5 are characterized in this work. Transitioning from step 5 to step 6, a possible untwisting of the right-hand tilted Mcm proteins in the double hexamer may locally unwind the dsDNA. Further modification by DDK and CDK and binding to Cdc45 and GINS lead to the separation of the double hexamer and formation of two CMG complexes each encircling ssDNA (step 6).

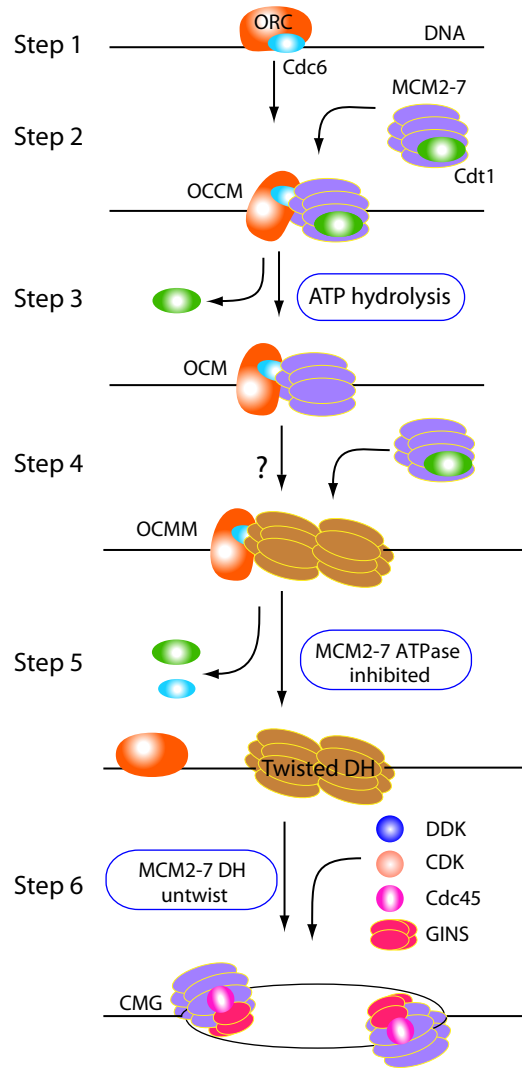


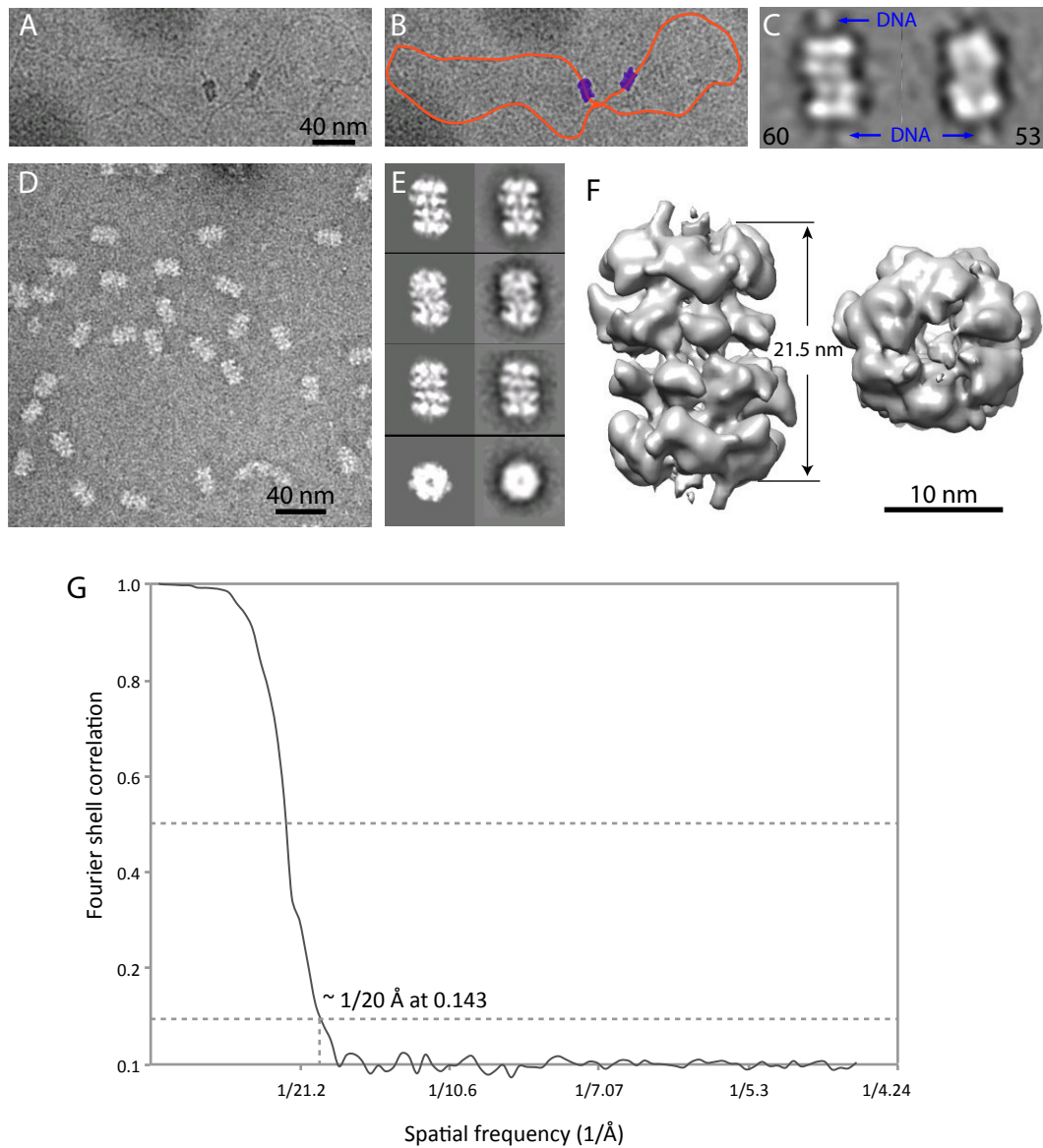




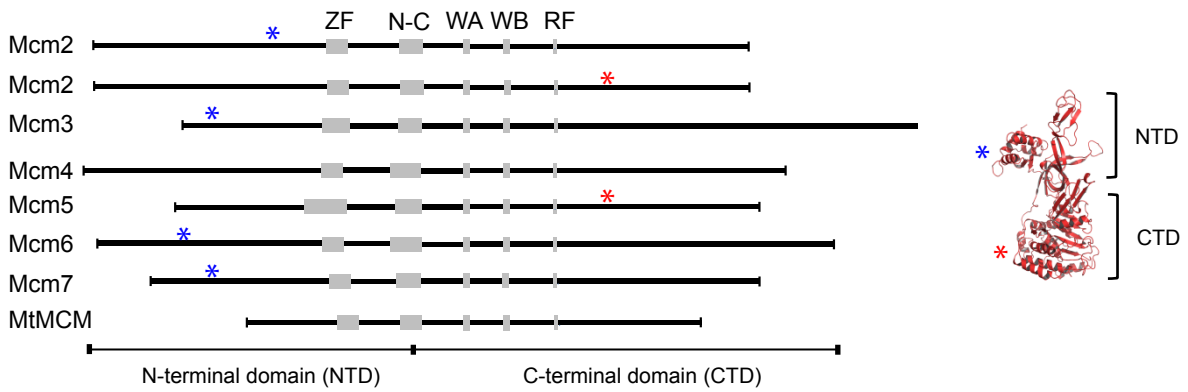


Sun_Fig6

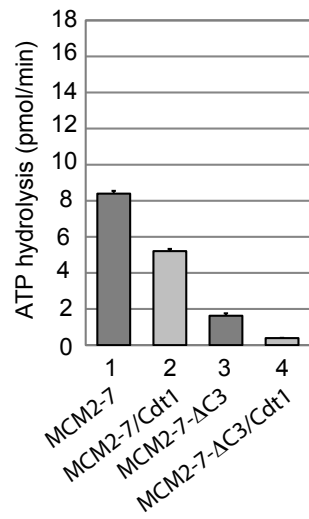




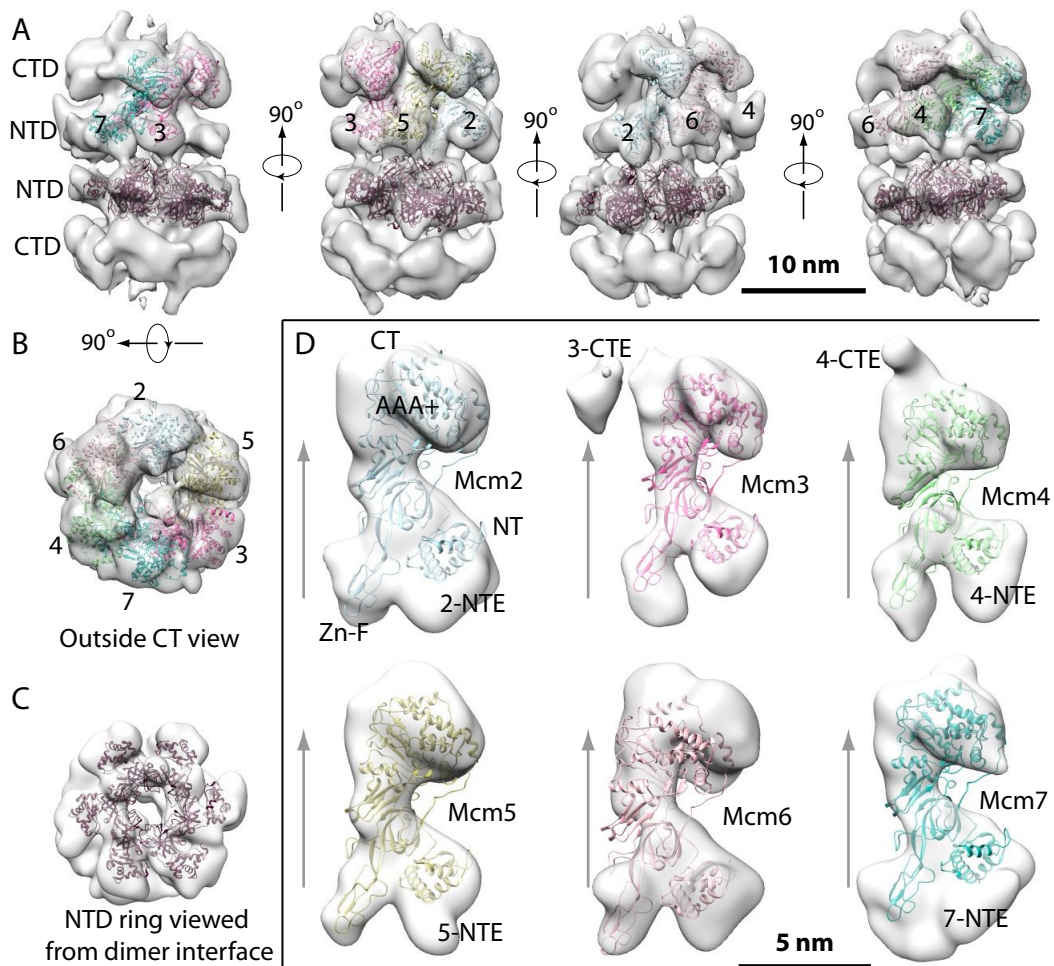
Supplementary figure 1. EM characterization and 3D reconstruction of in vitro assembled yeast Mcm2-7 double hexamer on a plasmid DNA. (A) A region of a cryo-EM micrograph showing two Mcm2-7 double hexamers assembled on a circular plasmid DNA. (B) A copy of (A) with DNA traced in orange and Mcm2-7 double hexamer shaded in purple. (C) Two class averages of the cryo-EM images of the Mcm2-7 double hexamers on intact plasmid. Blue arrows point to the DNA density on top or bottom of the double hexamer. Box size is 36 nm. Number at the lower corner indicates particles used to generate the class average. (D) Raw EM image of negatively stained Mcm2-7 double hexamers cleaved from the plasmid DNA by DNase I treatment. (E) Selected re-projections of the 3D reconstruction (left) and the approximately corresponding reference-free class averages of the negative-stain EM images of the Mcm2-7 double hexamer (right). Box size is 36 nm. (F) 3D negative-stain EM map of the Mcm2-7 double hexamer in side (left) and top (right) views. (G) The gold standard Fourier shell correlation curve suggests a resolution of 2 nm for the 3D EM density map of the in vitro assembled and purified yeast Mcm2-7 double-hexamer.



Supplementary figure 2. Schematics of the *S. cerevisiae* Mcm2-7 proteins. The conserved zinc-fingers (ZF), N/C-terminal linker, WA, WB and arginine-finger (RF) motifs are indicated. The archaeal *S. solfataricus* MCM crystal structure is shown as an example of a MCM protein (PDB: 3F9V). The asterisks mark the MBP insertion positions.

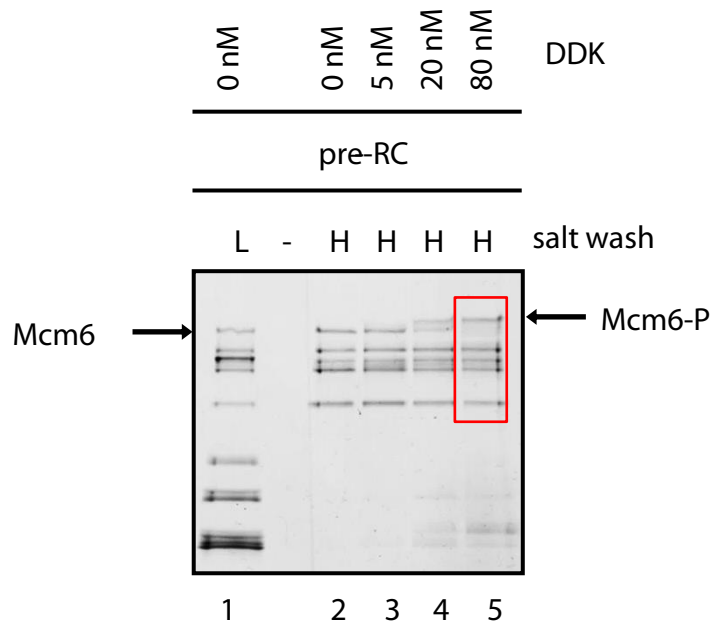


Supplementary figure 3. ATPase activities of wild type and mutant Mcm2-7 hexamers. Mcm2-7-Δ3C has much reduced ATPase activity (lane 3), which is further suppressed by Cdt1 (lane 4).

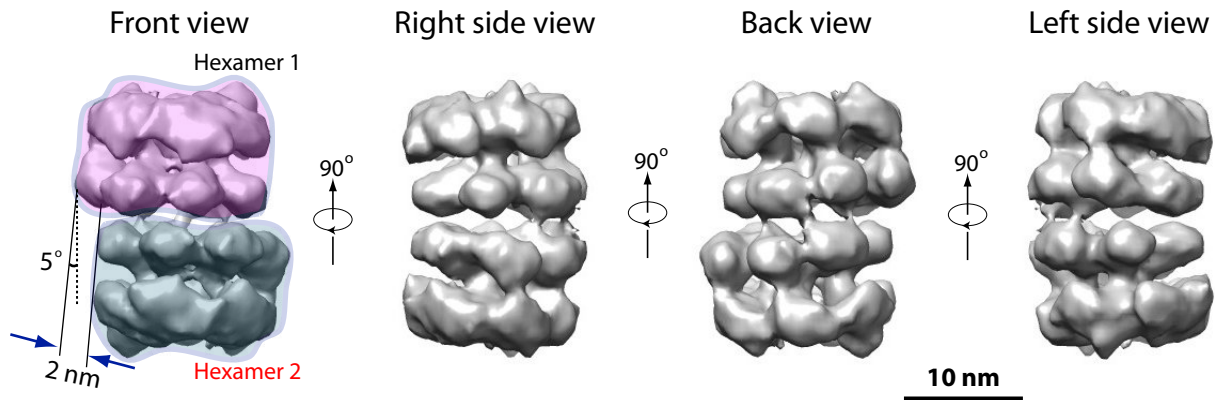


Supplementary figure 4. Docking of Archaeal MCM crystal structures into the 3D EM map of yeast Mcm2-7 double hexamer. (A) Four consecutively 90° rotated views of the Mcm2-7 double hexamer around a vertical axis. In the top Mcm2-7 hexamer density, two or three Archaeal MCM monomer crystal structures are docked as rigid bodies (PDB ID: 3F9V), as labeled by the MCM subunit numbers. In the bottom Mcm2-7 hexamer, the crystal structure of N-terminal domain hexamer of an Archaeal MCM is docked as a single rigid body (PDB ID: 1LTL). (B) Top, outside, and C-terminal view of 3D EM map of the Mcm2-7 double hexamer docked with six monomeric Archaeal MCM crystal structures (PDB ID: 3F9V). MCM subunit number is labeled. (C) Dimer interface and N-terminal view of the EM map of the bottom Mcm2-7 hexamer docked with the crystal structure of the N-terminal hexamer of the Archaeal MCM (PDB ID: 1LTL). The six N-terminal domains of the yeast MCM proteins are larger than the Archaeal counterpart, as demonstrated by the partially occupied EM densities. Panels A - C are on same scale. (D) Structures of the six segmented MCM protein densities each rigid-body docked with the Archaeal MCM monomer crystal structure (PDB ID: 3F9V). The Archaeal crystal structure lacks the last C-terminal helical domain. The vertical gray arrows indicate the central channel position of the Mcm2-7 double hexamer. NT, N-terminus; CT, C-terminus; CTE, C-terminal extension; Zn-F, Zn finger domain.

A



B



Supplementary figure 5. Surface-rendered 3D EM map of the DDK-modified wild type yeast Mcm2-7 double hexamer. **(A)** Pre-RC reactions washed with low salt (lane 1) or high salt (lanes 2-5) were incubated with 0 nM DDK (lanes 1 and 2), 5 nM DDK (lane 3), 20 nM DDK (lane 4) or 80 nM DDK (lane 5). The reaction that showed efficient phosphorylation by DDK (80 nM DDK – lane 5), as judged by the phosphor-shift of Mcm6, was used for electron microscopy. **(B)** The four panels show consecutively 90° rotated side views of the EM structure. The two hexamers are staggered by ~ 2 nm and tilted by ~ 5° respect to the vertical cylindrical axis. These features are essentially the same as the wild type double hexamer structure without the DDK-mediated phosphorylation. Density segmentation and subunit assignment are not attempted because MBP mapping was not performed on the DDK phosphorylated double hexamer.